Draft version December 15, 2019
Typeset using LaTeX **preprint** style in AASTeX61

PHOTOMETRIC PROPERTIES OF THE RR LYRAE STAR SS PISCIUM

Matthew Murphy,[1] Tyler Nill,[1] and Brianna Isola[1]

[1] *Department of Physics & Astronomy, Stony Brook University, Stony Brook, NY*

ABSTRACT

RR Lyrae stars have long served as standard candles in astronomy. These stars exhibit periodic brightness variations. This variation is related to the star's intrinsic luminosity and its light curve can be parameterized to estimate stellar properties. We present photometric observations of the type C RR Lyrae star SS Piscium, spanning three nights. Observations were taken from the 14-in telescope of Mt. Stony Brook Observatory. We have created a composite light curve and have measured a variation period of $T = 0.292 \pm 0.002$ days. From a Fourier decomposition of this light curve, we determined the star's iron abundance (using the Zinn & West scale) to be $[\mathrm{Fe/H}] = -0.896 \pm 0.181$ and the heliocentric distance to be $d = 984.7 \pm 70.3$ pc. Our period measurement agrees with previous literature to within 2σ. Our measurement of the iron abundance is consistent within 0.5σ and confirms the status of SS Psc as being metal-strong compared to other RR Lyrae stars.

1. INTRODUCTION

RR Lyrae stars are a class of periodic variable stars. Observations of RR Lyraes began in the early 1890s when astronomers began to find variable stars in globular clusters. In fact, the majority of these stars identified today lie within globular clusters. However, these stars were initially lumped together with Cepheid variables. It was not until around 1915-1930 that RR Lyrae stars were realized to belong to their own class, separate from Cepheids (Smith 1995).

RR Lyrae stars are typically found to lie on the horizontal branch. They are less massive than the Sun, ranging from 0.5 - 0.8 solar mass. It is theorized that these stars burn helium at their core (Smith 2013), and their variation is a result of radial pulsations. The RR Lyrae class is subdivided into three main types: RRab, RRc, and RRd. Each type differs in the behavior of its brightness variation. RRab stars are the most common, accounting for about 91% of observed RR Lyrae. These are active in the fundamental mode of pulsation. Their light curves exhibit quick, steep increases and decreases in brightness, followed by periods of constancy. RRc stars make up about 9% of the class. These are active in the first overtone of pulsation. They exhibit continuous brightness variations that typically take on a sinusoidal shape. RRc variations usually have shorter periods than RRab (Smith 1995). The RRd type is far more rare than the other two. These stars are active in both the fundamental mode and first overtones, and exhibit double-mode variations (Soszyński et al. 2016).

RR Lyrae stars are valuable observables since they act as standard candles. A standard candle is an object whose luminosity can be determined from observable properties. Comparing the object's observed brightness with its intrinsic brightness is a direct measure of its distance. In the case of RR Lyrae stars, the period of their brightness variation is related to the star's luminosity. Their prevalence in globular clusters allows for probing of distances to these clusters within the Milky Way. The properties of an RR Lyrae class star are encoded in its light curve.

Ferro et al. (2012) have shown that the V-band light curve of an RR Lyrae star can be fit with a Fourier series of the form

$$m_V = a_0 + \sum_{n=1}^{N} a_n \cos\left(2\pi n x + \phi_n\right), \tag{1}$$

where $x \equiv (t - t_0)/T$. Here, t_0 represents the epoch of maximum brightness. This is simply a reference time when the star's magnitude reaches a maximum. The period of variation is T and a_n and ϕ_n are fitting parameters. Ratios in these Fourier phases are defined as $\phi_{jk} \equiv k\phi_j - j\phi_k$.

RRc stars are particularly practical for this analysis. Their sinusoidal light curves maximize the usefulness of this Fourier treatment. The stellar properties encoded in the light curve are uncovered by the Fourier parameters and the period of variation. For RRc stars, Kovács & Kanbur (1998) have shown that the absolute visual magnitude can be obtained as

$$M_V = -0.961T - 0.044\phi_{21} + 4.447a_4 + 1.061. \tag{2}$$

With the observed apparent visual magnitude and the calculated absolute magnitude from (2), one can calculate the distance in parsecs to the star:

$$d = 10^{\frac{m_V - M_V + 5}{5}}. \tag{3}$$

The star's metallicity can also be inferred from this Fourier decomposition. Morgan et al. (2007) have fit the iron-abundance of RRc stars to the relation

$$[Fe/H] = 52.466T^2 - 30.075T + 0.131\phi_{31}^2 + 0.982\phi_{31} - 4.198\phi_{31}T + 2.424. \tag{4}$$

Here, the iron abundance uses the Zinn & West metallicity scale (Zinn & West 1984). All abundances presented hereafter will be on this scale.

The variation periods of RR Lyrae stars remain relatively constant. Measurements of globular cluster RR Lyrae stars by Catelan (2009) show that the majority of these stars have period changes of less than 0.05 days per million years. Period change is most commonly and most strongly observed in RRab stars, whereas RRc stars exhibit little to no change. Based on this, we reason that the variation period and parameters determined from an RRc light curve will remain roughly constant over timescales from hundreds to millions of years. Therefore, the stellar properties determined from these parameters are accurate representations of the star at any given time and should not vary intrinsically between observations.

One particulary interesting RRc star is SS Piscium (SS Psc). The true nature of this star has been under recent debate. Different sources have classified it as either a high-amplitude δ Scuti variable (Antonello et al. 1986) or an RRc variable (Kholopov 1987). An analysis of the star's Fourier phases by Ferro et al. (2012) favors the RRc classification, and the majority of recent surveys (Gavrilchenko et al. (2014), Gaia Collaboration et al. (2017), Marsakov et al. (2018)) classify it as such. We will follow suit and treat the star as an RRc variable. The star is listed as an RRc in the Northern Sky Variability Survey catalogue with a variation period $T = 0.287$ day (Wils et al. 2006). Its relatively short period amongst RR Lyrae stars makes it a practical observing target for photometric measurements. The spectral range of SS Piscium is A7-F2 (Ferro et al. 2012). Therefore, we expect its T_{eff} to be roughly within 6000 - 7400K. As a blackbody, this peaks in the visible spectrum.

In this work, we focus on SS Piscium. In section 2 we describe our observational setup and techniques for taking photometric measurements of this star. We describe the necessary image reduction and present our measurement of the system's lightcurve in section 3. The analysis of this light curve is detailed in section 4 and our results are interpreted with respect to previous literature in section 5. We have also included an appendix containing further information on our observing targets and the light curve fitting.

2. DATA ACQUISITION

2.1. *Observing Equipment*

Observations were made using the 14-inch Meade LX200-ACF telescope operated by the Stony Brook University Department of Physics & Astronomy. This is a ground based telescope in Stony Brook, NY, USA. The telescope was equipped with a SBIG STL-1001E CCD set to its imager camera. The CCD was set to a temperature of $T_{CCD} = -10.0°C$ which was maintained to within $\pm 0.4°C$ throughout all observations. In previous work with this CCD, we have shown that this temperature setting reduces dark current to less than 1.635 $e^-/p/s$ (Murphy et al. 2019).

The spectrum of SS Piscium peaks in the visual, and the analysis of RRc stars as presented in section 1 relies on V-band measurements. This makes observing optimal for our CCD equipped with its V-band filter.

2.2. *Observing Runs*

Observations were made on three separate nights: Oct. 28, 2019, Nov. 4, 2019, and Nov. 6, 2019, local time. The first night was ended early due to heavy cloud cover, and its details are listed in Table 1. The second night had heavy cloud cover during the middle of the observing period, and its

details are listed in Table 2. Our time using the telescope on the third night was split with another research group doing a separate project. That night's details are listed in Table 3.

Table 1: Record of imaging for the first night of observing. Images with listed time prior to 00:00UT correspond to Oct. 28, 2019 (UT) and those after 00:00UT correspond to Oct. 29, 2019 (UT).

Image/Target	Start Time (UT)	End Time (UT)	N_{exp}	Exposure [s]	Filter	AutoDark Reduction
Flat-field	22:45	22:46	10	4.5	V	Applied
Dark Frame	03:05	03:10	10	27	V	None
SS Psc	23:50	03:00	359	27	V	None

Table 2: Record of imaging for the second night of observing. Images with listed time prior to 00:00UT correspond to Nov. 4, 2019 (UT) and those after 00:00UT correspond to Nov. 5, 2019 (UT).

Image/Target	Start Time (UT)	End Time (UT)	N_{exp}	Exposure [s]	Filter	AutoDark Reduction
Flat-field	22:34	22:35	10	5.5	V	Applied
Dark Frame	07:22	07:25	10	20	V	None
	07:27	07:30	10	15	V	None
SS Psc	00:47	05:52	1-914	15	V	None
	05:59	07:20	915-1114	20	V	None

Table 3: Record of imaging for the third night of observing. Images with listed time prior to 00:00UT correspond to Nov. 6, 2019 (UT) and those after 00:00UT correspond to Nov. 7, 2019 (UT). The set of dark frames with 25s exposures had to be retaken on a later date due to an unknown corruption of the original images.

Image/Target	Start Time (UT)	End Time (UT)	N_{exp}	Exposure [s]	Filter	AutoDark Reduction
Flat-field	23:36	23:37	10	0.3	V	Applied
Dark Frame	06:39	06:42	10	15	V	None
			14	25	V	None
SS Psc	00:05	01:59	1-231	25	V	None
	02:03	03:03	232-307	15	V	None
	05:40	06:38	307-484	15	V	None

The CCD was set to use 1x1 image binning. All flat-fields were dome-flats taken with AutoDark reduction. The dark frames and target images had this reduction turned off. The exposure times were chosen to avoid saturating the CCD, which occurs at $\approx$ 65,000 counts per pixel. The exposure

time was adjusted as necessary to keep the target count levels at $\approx 10-15\%$ of the saturation value and that of the brightest stars in the image at $\approx 40\%$ of the saturation value, at most.

3. DATA REDUCTION

3.1. *Image Correction*

We first treated each night's data separately for ease of organization. Each set of dark frames was median combined into a master dark frame. The master dark frame is subtracted from the target images of corresponding exposure time. Similarly, each night's set of flat-fields were combined into master flat fields. These master flat frames were normalized with respect to that frame's mode count value. The resulting pixel values were spread about 1.0 near the image center and about 0.95 toward the edges, reflecting the non-uniform sensitivity across the CCD. The dark corrected target images were divided by that night's corresponding normalized master flat field, which corrects for the non-uniformity.

We solved for the WCS of each target image using a local copy of the Astrometry.net [1] service. The light from SS Psc was encompassed within an image aperture of 18, 15, and 17 pixels diameter on images from the first, second, and third night, respectively. These aperture sizes were chosen to contain most of the target's light and be robust against seeing variations. They are larger than that which optimizes the SNR. The flux of each source within this aperture on each image was measured using the Source Extractor [2] software.

We extracted the flux and corresponding error for our target SS Psc and seven other reference stars. The name and coordinates of each star is listed in Table 9 and their relative positions on a sample image is shown in Figure 3. One of these reference stars is HD 8109, which we will hereafter refer to as our magnitude calibrator. This star has a visual magnitude $m_V = 8.86$, taken from the Simbad database [3]. We will use this star to calculate the visual magnitude of SS Psc. The other reference stars will be used to calibrate the flux data of SS Psc and HD 8109 for atmosphere effects.

3.2. *Lightcurve Calibration*

We have analyzed each night's data separately. We scale each reference star's flux f_j and the error on the flux σ_{f_j} by that star's average flux $\langle f_j \rangle$ over the observing period. This scales each star's signal to scatter around 1.0, so that we may average them.

Our observations were heavily affected by cloud cover and near-overcast weather. For the first night's set of data, 25 exposures were rejected at the end before observations were terminated. The second night was most affected, with 44% of exposures needing rejection from analysis due to clouds. The third night had clear skies and no exposures were rejected. However, we encountered technical issues that limited the amount of data taken.

Our CCD has a $24'$ field of view. Each star was near the center of this FOV so they were all confined within a relatively small area on the sky. Therefore, it is assumed that any atmospheric or seeing variations will have affected each star on the image equally. We account for any such variations by scaling the signals from SS Psc and HD 8109 to the weighted mean of the reference stars. For each i^{th} image, we compute the weighted mean μ_i^{ref} and its corresponding error σ_i^{ref} of the scaled flux measurements of the j reference stars.

[1] http://astrometry.net/
[2] http://www.astromatic.net/software/sextractor
[3] http://simbad.u-strasbg.fr/simbad/sim-id?Ident=HD+8109

$$\mu_i^{ref} = \frac{\sum_j f_j^{ref} / \left(\sigma_j^{ref}\right)^2}{\sum_j 1 / \left(\sigma_j^{ref}\right)^2} \tag{5}$$

$$\sigma_i^{ref} = \sqrt{\frac{1}{\sum_j 1 / \left(\sigma_j^{ref}\right)^2}} \tag{6}$$

This weighted mean takes in account the statistical weight of each star when averaging on each image. This reduces statistical noise and any systematic uncertainty due to undetected variability in brightness. Since we assume that atmospheric effects will have disrupted each star's signal equally, scaling the flux of our target and magnitude calibrator effectively eliminates these adverse effects on the measurement. We calculate this scaling as $r_i = f_i^{SS}/\mu_i^{ref}$ for the flux f_i^{SS} of SS Psc and $r_{c,i} = f_i^{HD}/\mu_i^{ref}$ for the flux f_i^{HD} of HD 8109.

Next, we calculate the magnitude m_V of SS Psc at each exposure using the relation

$$m_{V,i} = m_{HD8109} - 2.5 \log_{10}\left(\frac{r_i}{r_{c,i}}\right). \tag{7}$$

Since the magnitude calculation depends only on the ratio of fluxes, the units do not matter. We used the scaled fluxes. The error on the magnitude is calculated as

$$\sigma_{m_{V,i}} = \sqrt{\sigma_{m_{HD}}^2 + \left(\frac{\partial m_{V,i}}{\partial(r_i/r_{c,i})}\right)^2 \sigma_{r_i/r_{c,i}}^2}, \tag{8}$$

by following standard error propagation methods. The result is three separate light curves for each night of observations, as seen in Figure 1.

To perform a Fourier decomposition, we first combine these three sets of data. To do so, we shift the sets by a multiple of the light curve period. The second and third night's data, shown in Figures 1b and 1c respectively, each show the expected sinusoidal behavior. We can estimate the period of variation for each set by fitting them separately to the form

$$m_V(t) = A \sin\left(\frac{2\pi}{T} t + \psi\right) + C. \tag{9}$$

Here, A is the amplitude, ψ is the phase, and C is an offset. We performed this using the MATLAB Curve Fitting Toolbox [4], which minimizes the root mean square error and optimizes the R-square value. The best fit gives $T_{n2} = 0.298 \pm 0.005$ day for the second night and $T_{n3} = 0.314 \pm 0.002$ day for the third night. Averaging these values gives an estimate for the period of $T_{fit} = 0.3$ day.

On the first night of observing, we found a brightness maximum at Julian date $t_{0,1} = 2458785.531 \pm 0.003$. On the second night, we observed another maximum at $t_{0,2} = 2458792.730 \pm 0.005$. On the third night, we observed another at $t_{0,3} = 2458794.746 \pm 0.003$. The error on these epoch times comes from scatter around the maximum, creating difficulty in determining its exact time.

[4] https://www.mathworks.com/products/curvefitting.html

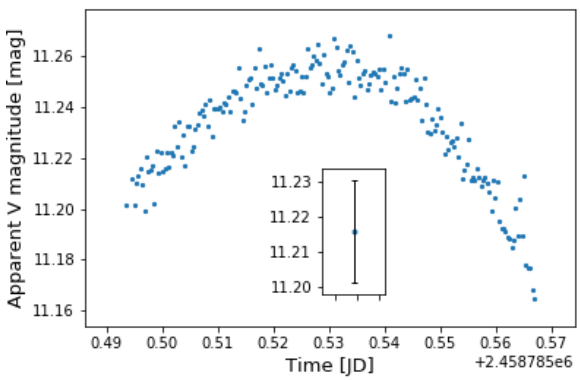

(a) Night 1

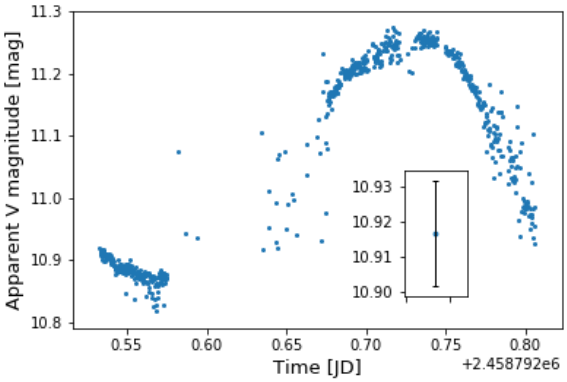

(b) Night 2

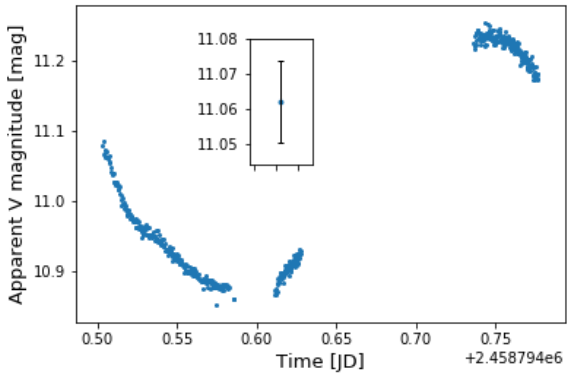

(c) Night 3

Figure 1: Magnitude light curves of SS Piscium on three separate nights of observing. These observations were made with the 14-in telescope at Stony Brook University. These nights in order, 1a, 1b, and 1c, are Oct. 28, 2019, Nov. 4, 2019, and Nov. 6, 2019, respectively. Error bars are not shown on each point for better visualization. The subplot on each figure shows the typical error on the magnitude for that night's set of data. This error never exceeded 0.02 mag.

We will keep the third night's data fixed on its axes and shift the first two sets forward in time. The number of periods N_i that each set must be shifted forward by is calculated as

$$N_1 = \frac{t_{0,3} - t_{0,1}}{T_{fit}} - 2, \tag{10}$$

$$N_2 = \frac{t_{0,3} - t_{0,2}}{T_{fit}} - 1. \tag{11}$$

Subtracting 2 and 1 respectively keeps the composite curve in phase. Otherwise, they would just stack on top of one another. We then iterate the data from night 1 forward by $N_1 T_{fit}$ and the data from night 2 forward by $N_2 T_{fit}$.

Since we have iterated the sets forward in time, each point now lies at an adjusted time $t_{adj} = t_{original} + N_i T_{fit}$. We must redefine the time axis. We use the first maximum as a reference point, which now lies at $t_{adj,0} = t_{0,1} + N_1 T_{fit}$. We calculate $x = (t_{adj} - t_{adj,0})/T_{fit}$ for each point. The result

is a composite magnitude light curve of all three nights' data. The magnitude is now varying with x, which appears as the argument in (1). We plot this composite curve in Figure 2.

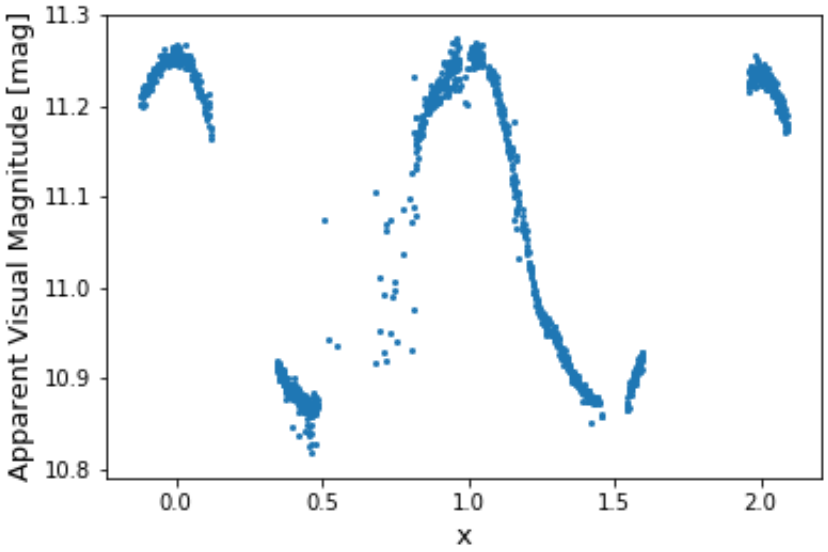

Figure 2: Composite magnitude light curve of SS Piscium, constructed from the three separate observing nights shown in Figure 1. The data was iterated by multiples of the variation period to create this curve. We see the sinusoidal behavior expected from an RRc variaton (Smith 1995), and seem to have observed three brightness maxima. The y-axis gives the apparent visual magnitude m_V. We plot the magnitude against x, which will be used to fit a Fourier series to this light curve.

4. ANALYSIS OF SS PSC

Fitting the light curve in Figure 2 to the sinusoidal form in (9) returns a best-fit period of $T = 0.292 \pm 0.002$ day. We will use this period value in our Fourier treatment. We fit the same light curve to the Fourier series in (1). This was also performed using the MATLAB Curve Fitting Toolbox. Following Ferro et al. (2012), we take the series out to four terms. The resulting parameter values are listed in Table 4. This returns a root mean square error of 0.01807 and an R-square value of 0.9865, so it is a good fit. An overlay of this fit onto our light curve can be seen in Figure 4.

Table 4: Parameters obtained from fitting a 4-term Fourier series, as in (1), to the light curve of SS Piscium

	a_0	a_1	a_2	a_3	a_4	ϕ_1	ϕ_2	ϕ_3	ϕ_4
Value	11.04	0.191	0.025	0.00108	0.0124	0.1565	-6.29	4.3	3.55
Error	0.01	0.001	0.002	0.00174	0.0016	0.0147	0.08	2.1	0.15

4.1. *Heliocentric Distance*

From the values in Table 4, we can calculate the phase $\phi_{21} = \phi_2 - 2\phi_1 = -6.60 \pm 0.09$. Plugging this, our value of the period T, and the value of a_4 from the table into (2) gives the value of the absolute visual magnitude. We calculate $M_V = 1.13 \pm 0.01$.

The absolute magnitude is like a measure of the star's luminosity. The difference between the star's intrinsic brightness and its observed brightness is a direct measure of how far away it is. To determine the distance using (3), we must obtain a single value for the apparent magnitude. We simply calculate the average magnitude in the m_V versus x light curve, giving $m_V = 11.09 \pm 0.15$. The distance equation in (3) is defined in units of parsecs. Plugging in our values gives a heliocentric distance to SS Psc of $d = 984.7 \pm 70.3$ *pc*.

4.2. *Metallicity*

From Table 4, we calculate the phase $\phi_{31} = \phi_3 - 3\phi_1 = 3.83 \pm 0.23$. Plugging this and our value for T into (4) gives an iron abundance of $[\mathrm{Fe/H}] = -0.896 \pm 0.181$.

5. DISCUSSION

We have constructed a magnitude light curve of SS Piscium from three nights of observations, as plotted in Figure 2. From this light curve, we have determined the star's visual magnitude, variation period, distance, and metallicity (on the Zinn & West scale).

Let's first check our measurement of the visual magnitude. Our measurement is listed amongst literature values in Table 5. We see that our determination is in excellent agreement with literature. The largest discrepancy is by 0.7σ from the value reported by Dambis et al. (2013), but this is not significant.

Table 5: Visual magnitude determination of SS Psc and literature comparisons.

	This work	Dambis et al. (2013)	Høg et al. (2000) [a]	Gaia Collaboration et al. (2017)
m_V [mag]	11.09	10.98	11.01	10.98
error [mag]	0.15	0.01	0.07	0.02

[a]Tycho-2 Catalogue

Let's next check our determination of the star's variation period. We list our determination alongside several literature values in Table 6. Our measurement of the variation period is longer than that of Ferro et al. (2012) and Wils et al. (2006), but is still consistent to within 1.6σ. It is also consistent with the value listed by Gavrilchenko et al. (2014) to within 0.33σ. As discussed in Catelan (2009), the actual period will not have changed significantly in the time periods between our observations and those of other groups. The agreement between our period value and that of literature confirms this on a very short timescale (tens of years).

Our determination of the star's iron abundance is listed in Table 7 alongside literature values. We find excellent agreement with Ferro et al. (2012) to within 0.05σ. Our measurement is also very consistent to within 0.5σ of Norris (1986), and this is without having found a reported error on their measurement.

We have confirmed that SS Piscium is metal-strong compared to other globular cluster RR Lyrae stars. It is more metal rich than most other RR Lyrae stars, whose abundances typically range

Table 6: Variation period determination of SS Psc and literature comparisons.

	This work	Ferro et al. (2012)	Gavrilchenko et al. (2014) [a]	Wils et al. (2006) [b]
T [day]	0.292	0.288712	0.302	0.2878
error [day]	0.002	0.000005	0.011	

[a]Wide-field Infrared Survey Explorer
[b]Northern Sky Variability Survey

between $-2.0 <$ [Fe/H] < -1.0 (Marsakov et al. 2018). Both Ferro et al. (2012) and McNamara & Redcorn (1977) further discuss the star having a spectrum rich in metal lines, though our measurements can not confirm this.

Table 7: Iron abundance determination of SS Psc and literature comparisons.

	This work	Ferro et al. (2012)	Norris (1986)
[Fe/H] [sun]	-0.896	-0.88	-0.82
error	0.181	0.21	

Finally, we list our calculation of the star's distance from the Sun alongside compiled literature values in Table 8. Our measurement agrees well with the value listed by Marsakov et al. (2018) and is within about 1σ of both Gavrilchenko et al. (2014) and the value computed from the parallax reported in Gaia Collaboration et al. (2017).

RR Lyrae stars are most commonly found in globular clusters. As a result, these stars are typically used as standard candles to probe galactic globular clusters. We are unsure of SS Piscium's placement in any globular cluster. Based on a listing [5] of known globular clusters within the Milky Way, the combination of SS Psc's coordinates and distance seem to place it outside of any globular cluster. However, this list compiles the distances and coordinates of only the 157 globular clusters identified up to 2011. Many new candidates have been identified since 2012 and are listed without coordinates or distances, so we can not definitively remark on the location of SS Piscium. If it is outside a globular cluster, it would be unusual for an RR Lyrae star and would complement the star's status as a peculiar RRc star, as discussed in Ferro et al. (2012). We have not found any previous literature remarking on SS Piscium being in a particular cluster.

Table 8: Distance determination to SS Psc and literature comparisons.

	This work	Gavrilchenko et al. (2014)	Gaia Collaboration et al. (2017) [a]	Marsakov et al. (2018)
d [pc]	984.7	1083	900.9	959
error [pc]	70.3	20	40.6	

[a]Computed from the reported trigonometric parallax

[5] http://www.messier.seds.org/xtra/supp/mw_gc.html

6. CONCLUSION

We conducted a three night photometric observation of the RRc star SS Piscium. A composite light curve was created using each night's data, as seen in Figure 2. We measured a visual magnitude of $m_V = 11.09 \pm 0.15$, which is consistent with literature measurements. We measured a variation period of $T = 0.292 \pm 0.002$ days and an iron abundance of $[\mathrm{Fe/H}] = -0.896 \pm 0.181$. Our value for the period is longer than but still in agreement with that of Ferro et al. (2012). Our value for the iron abundance is highly consistent with theirs and that of Norris (1986). This indicates that SS Piscium is metal strong compared to other RR Lyrae stars. Lastly, we measured a distance of $d = 984.7 \pm 70.3$ pc to the star. This may place the star outside of a globular cluster, but more information on the positions of Milky Way globular clusters is needed.

REFERENCES

Antonello, E., Broglia, P., Conconi, P., & Mantegazza, L. 1986, A&A, 169, 122

Catelan, M. 2009, Ap&SS, 320, 261, doi: 10.1007/s10509-009-9987-8

Dambis, A. K., Berdnikov, L. N., Kniazev, A. Y., et al. 2013, MNRAS, 435, 3206, doi: 10.1093/mnras/stt1514

Ferro, A. A., Pena, J. H., & Jaimes, R. F. 2012, Physical parameters of three field RR Lyrae stars. https://arxiv.org/abs/1210.7886

Gaia Collaboration, Clementini, G., Eyer, L., et al. 2017, A&A, 605, A79, doi: 10.1051/0004-6361/201629925

Gavrilchenko, T., Klein, C. R., Bloom, J. S., & Richards, J. W. 2014, MNRAS, 441, 715, doi: 10.1093/mnras/stu606

Høg, E., Fabricius, C., Makarov, V. V., et al. 2000, A&A, 355, L27

Kholopov, P. N. 1987, General Catalogue of Variable Stars.

Kovács, G., & Kanbur, S. M. 1998, Monthly Notices of the Royal Astronomical Society, 295, 834, doi: 10.1046/j.1365-8711.1998.01271.x

Marsakov, V. A., Gozha, M. L., & Koval, V. V. 2018, Astronomy Reports, 62, 50–62, doi: 10.1134/s1063772918010055

McNamara, D. H., & Redcorn, M. E. 1977, Publications of the Astronomical Society of the Pacific, 89, 61, doi: 10.1086/130072

Morgan, S. M., Wahl, J. N., & Wieckhorst, R. M. 2007, Monthly Notices of the Royal Astronomical Society, 374, 1421, doi: 10.1111/j.1365-2966.2006.11247.x

Murphy, M., Isola, B., & Nill, T. 2019, Dark Current of the STL1001 Imaging CCD, Available at https://github.com/mm-murphy/CCD-Calibration

Norris, J. 1986, ApJS, 61, 667, doi: 10.1086/191128

Smith, H. A. 1995, RR Lyrae Stars (Cambridge University Press)

—. 2013, Period Changes of Mira Variables, RR Lyrae Stars, and Type II Cepheids. https://arxiv.org/abs/1310.0533

Soszyński, I., Smolec, R., Dziembowski, W. A., et al. 2016, Monthly Notices of the Royal Astronomical Society, 463, 1332–1341, doi: 10.1093/mnras/stw1933

Wils, P., Lloyd, C., & Bernhard, K. 2006, Monthly Notices of the Royal Astronomical Society, 368, 1757–1763, doi: 10.1111/j.1365-2966.2006.10236.x

Zinn, R., & West, M. J. 1984, ApJS, 55, 45, doi: 10.1086/190947

APPENDIX

Table 9: A listing of the target object and all reference stars used in the light curve analysis. The reference objects were identified using the CDS Portal at http://cdsportal.u-strasbg.fr/

Object	Identifier	RA [J2000]	Dec [J2000]
Target	SS Psc	01:20:52.36	+21:43:43.25
Magnitude Reference	HD 8109	01:20:53.99	+21:36:19.07
Reference 1	2MASS01204703+2137013	01:20:47.03	+21:37:01.35
2	TYC 1203-541-1	01:20:15.82	+21:36:50.83
3	TYC 1203-667-1	01:20:21.99	+21:43:48.84
4	2MASS01202661+2143558	01:20:26.61	+21:43:55.87
5	2MASS01203712+2149022	01:20:37.12	+21:49:02.22
6	2MASS01212316+2148422	01:21:23.17	+21:48:42.33

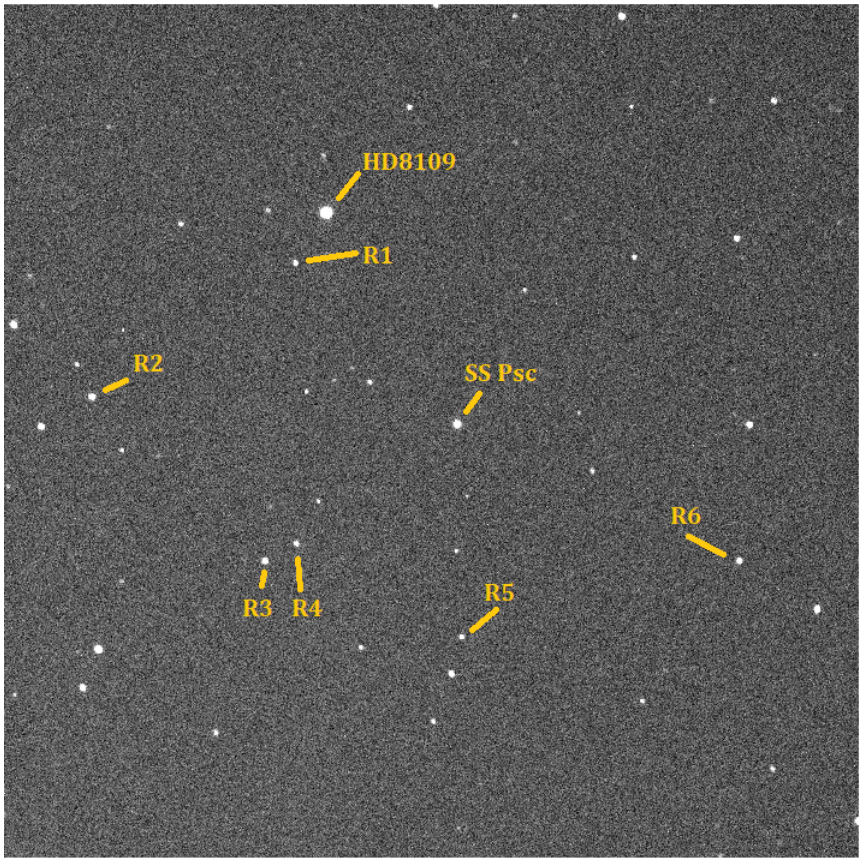

Figure 3: Here is an image taken on the third night of observation. The relative positions of the target SS Psc and all reference stars listed in Table 9 is shown.

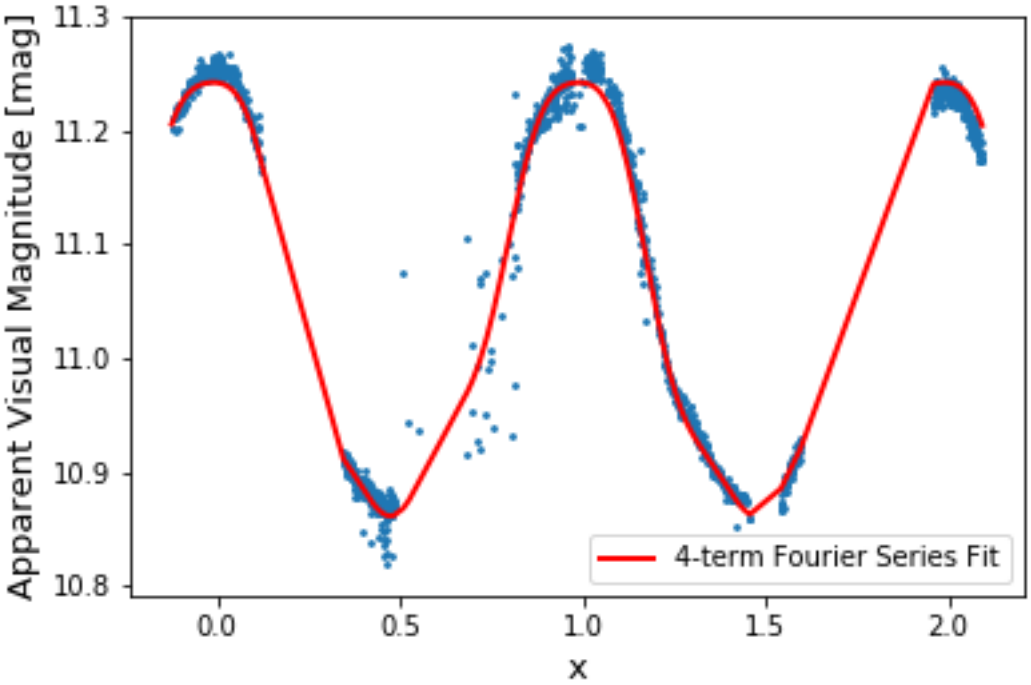

Figure 4: Here we overlay our composite light curve with its Fourier fit to demonstrate its effectiveness. The data points are the same as in Figure 2. The overlayed curve is a 4-term Fourier series, of the form given in (1), with the parameters listed in Table 4. We see that this Fourier decomposition does an excellent job at fitting our light curve with a root mean square error (RMSE) of 0.01807 and an R-square value of 0.9865. We performed this fitting using the MATLAB Curve Fitting Toolbox, available at https://www.mathworks.com/products/curvefitting.html, provided to us by Stony Brook University.